

High energy power-law tail in X-ray binaries spectrum and bulk Comptonization due to a conical outflow from a disk

Nagendra Kumar*

Department of Physics, Indian Institute of Science, Bangalore 560012, India †

Abstract

X-ray binaries (XRBs) often exhibit a high energy power-law tail (HEP-tail) and these tails can be generated by bulk Comptonization (BMC) process with a free-fall bulk region onto the compact object. The radio emission (which is generated by synchrotron-emitting outflowing electrons) is also observed in all spectral states of XRBs. Interestingly, the variation of HEP-tail flux in different spectral states is similar to the variation of radio flux. We motivate to study the HEP-tail in BMC process with an outflowing medium. For this we consider collimated and conical (of opening angle θ_b with axis perpendicular to the accretion disk) outflow geometries. We simulate the BMC spectrum by using a Monte Carlo scheme. We find that the emergent spectrum has power-law tail (of photon index $\Gamma > 2$ and with high energy cut-off $E_c > 200$ keV) only for $\theta_b \gtrsim 30$ degree in conical outflow, while for either collimated or conical (with $\theta_b < 30$ degree) outflow these HEP-tail can be only generated when it is also found in thermal Comptonized spectra (i.e., at sufficiently high medium temperature). We describe the observed GRS 1915+105 spectrum for two classes χ and γ in conical outflow, in both cases the estimated outflow speed is relativistic and the kinetic power of wind indicates that the HEP-tail can be generated at inner region of the accretion disk, like inner disk radio emission.

Key Words: stars: black holes – stars: neutron – X-rays: binaries – individual: GRS 1915+105 – radiation mechanisms: thermal

1 Introduction

Black hole (BH) low mass X-ray binaries (LMXBs) frequently change their X-ray spectral states particularly power-law dominated low intense hard (LH) state to blackbody dominated high intense soft (HS) state via outburst, which again settle down to the LH state. During the spectral state transition, sometimes a very high intense power-law dominated (VHS) state with photon index $\Gamma > 2.4$ is observed without an exponential high energy cut-off (E_c) and generally referred as a steep power law (SPL) state (for review see, McClintock & Remillard, 2006; Done et al., 2007). High energy power-law tail (hereafter, HEP-tail) is observed in both states LH and HS with $\Gamma > 2.0$, which usually extends up to ≥ 200 keV (or $E_c > 200$ keV) (e.g., McConnell et al., 2002; Motta et al., 2009; Titarchuk & Shaposhnikov, 2010), and it is also detected in neutron star (NS) LMXBs (e.g., Revnivtsev et al., 2014).

The low energy (2-100 keV) power-law component has been believed due to a thermal comptonization (TC) of a disk photons, but for the HEP-tail a modified version of TC has been invoked. Example, Done & Kubota (2006) assumed that the disk and Comptonizing medium are energetically coupled to each other (see also, Kubota & Done, 2016); in hybrid model a hybrid electrons velocity distribution (thermal + non-thermal [power law]) has been considered (Coppi, 1999; Gierliński et al., 1999) and in bulk Comptonization (BMC) model the electrons are in a free-fall converging flow of spherically accreted plasma into BH (Titarchuk et al., 1997, and for NS e.g., Farinelli et al., 2009).

In BMC framework, for a spherically diverging outflow, Laurent & Titarchuk (2007) had noticed only downscattering of the soft spectrum, i.e., the HEP-tail has not been generated in this model (see also, Psaltis, 2001; Ghosh et al., 2010). However, the outflow is observed in all spectral states of LMXBs, e.g., the radio jet outflow is in LH & SPL states, and wind outflow is in HS state (e.g., Fender & Belloni,

*E-mail:nagendra.bhu@gmail.com

†current address- Aazad Path, New Bengali Tola, Mithapur, Patna-800001

2012; Ponti et al., 2012; Díaz Trigo & Boirin, 2016; Degenaar et al., 2016; Miller et al., 2016). Wind and jet can exist simultaneously e.g., in LMXBs (Homan et al., 2016; Drappeau et al., 2017; Tetarenko et al., 2018), in active galactic nuclei (e.g., Tombesi et al., 2014). Morphologically, in some systems the inferred wind outflow geometry is a conical shape (e.g., Knigge et al., 1995; Tombesi et al., 2015; Degenaar et al., 2016). Although the radio emission is mainly associated to the LH and SPL states, but a fainter radio emission has been observed also in the HS state. In general the radio emission is generated at inner accretion disk by synchrotron emitting outflowing relativistic electron (e.g., Fender et al., 1999; Fender & Hendry, 2000; Fender & Kuulkers, 2001; Fender et al., 2004, 2009; Munro et al., 2001; Rushton et al., 2010). Interestingly, the HEP-tail flux in HS state is also comparatively smaller than the SPL state. Also, the jet power of SPL is positively correlated with peak X-ray luminosity of HS (e.g. Zhang & Yu, 2015). It might be possible that the emission mechanism of HEP-tail is related, in some sense, to the emission mechanism for radio emission. In present work, we attempt to describe the HEP-tail emission mechanism in outflowing medium in BMC framework. For outflowing medium we consider two geometries, conical and collimated outflow. We compute the spectrum by using a Monte Carlo method for BMC. We find that when the outflow is a conical type (i.e., at any scattering point P the electron's outflow/ bulk direction is any one of the directions inside the cone of opening angle θ_b at P) then the soft photons can get upscattered and the emergent spectrum has a power-law component. Energetic of wind outflow indicates that HEP-tail emission can be generated in inner region of the disk like radio emission.

2 Calculations and Results

Method : In bulk Comptonization, the photons are upscattered due to both thermal and bulk motions of the electron and it was initially formulated by Blandford & Payne (1981a,b). The average energy exchange per scattering ΔE for a monochromatic photon of energy E in the Comptonizing medium of temperature T_e and a constant bulk speed u_b (Titarchuk et al., 1997) is

$$\Delta E = \Delta E_{TH} + \left(\frac{4u_b}{c\tau} + \frac{(u_b/c)^2}{3} \right) \frac{E}{m_e c^2}. \quad (1)$$

Here, $\Delta E_{TH} = (4kT_e - E) \frac{E}{m_e c^2}$ is for thermal Comptonization (i.e., $u_b = 0$), τ is the optical depth of the scattering medium, m_e is the rest mass of the electron and k is Boltzmann constant. Since, the time averaged Comptonized spectrum depends on ΔE and the average number of scattering $\langle N_{sc} \rangle$ (e.g. Kumar & Misra, 2016a). Hence from equation (1), in general for a given $\langle N_{sc} \rangle$, the BMC spectrum would degenerate over kT_e and u_b . That is for a given BMC spectrum, at fixed $\langle N_{sc} \rangle$ the many sets of (kT_e, u_b) are possible that give same ΔE . We will verify the calculation results using it with considering one of set $(kT_e, u_b = 0)$ for TC (as for a special case the analytic solution for TC is known [Kumar & Misra e.g. 2016a, and references therein]), see Figure 5. We calculate the spectrum using a Monte Carlo (MC) method for BMC and the MC method has been described in appendix.

Calculation geometry : We assume that the outflow occurs on the accretion disk from the radius r to $r + W$, so the outflow region will be a torus shaped with a rectangular cross-section of width W . We assume, its height is L . The meridional cut of the torus is shown in Figure 1. We fix a global spherical polar coordinate (r, θ, ϕ) at the center of the torus (or at the compact object). Without loss of generality we assume, the torus exists only above the equatorial plane. The Compton scattering takes place inside the torus, we refer torus also as a Comptonizing medium or corona. We assume that the optical depth τ is along the vertical direction, and when the scattered photons cross the equatorial plane, these photons will get absorbed. The seed photon source is a blackbody at temperature T_b , which emits vertically from the equatorial plane of the accretion disk, and it is situated inside the torus. Depending on the $\frac{L}{W}$ ratio and the mean free path of photon inside the torus (λ , and here $\lambda \ll W$), the scattered photons can escape either from the top of the torus (1st case) or from the outer boundary of the torus (2nd case) or both. In which the 1st case dominates for $\frac{L}{W} \ll 1$. The 1st case is more relevant, in general, for XRBs, we consider only the 1st case for the calculation with taking $\frac{L}{W} = 0.1$.

For outflow geometry we consider two physical situations (a) collimated outflow, and (b) conical outflow. In collimated outflow, the electron's medium flows in θ_b direction (i.e., away from the compact object) with bulk speed u_b at any scattering point P on fixed ϕ -plane in the global coordinate as shown in the left side of Figure 1. In conical outflow, to assign the outflow direction we consider a cone of opening

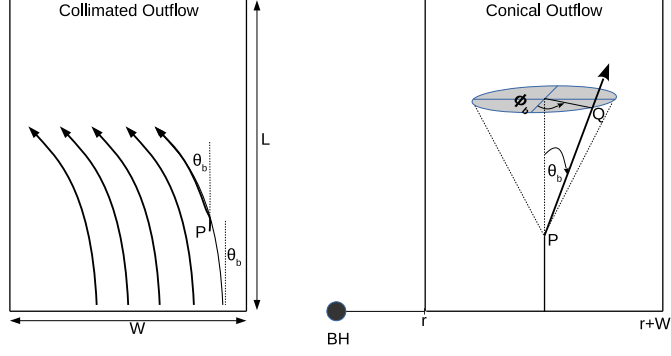


Figure 1: Meridional cut of a rectangular torus shaped Comptonizing medium (or corona) of width W and height L surrounding the BH to study the outflow motion. In left side, a schematic diagram for the collimated flow of angle θ_b has been shown. In right side we show a schematic diagram for the conical flow of opening angle θ_b . Here, the conic shaded region is for a possible conical outflow direction at the scattering point P , and the PQ is one of outflow direction (θ_b, ϕ_b) in local coordinate.

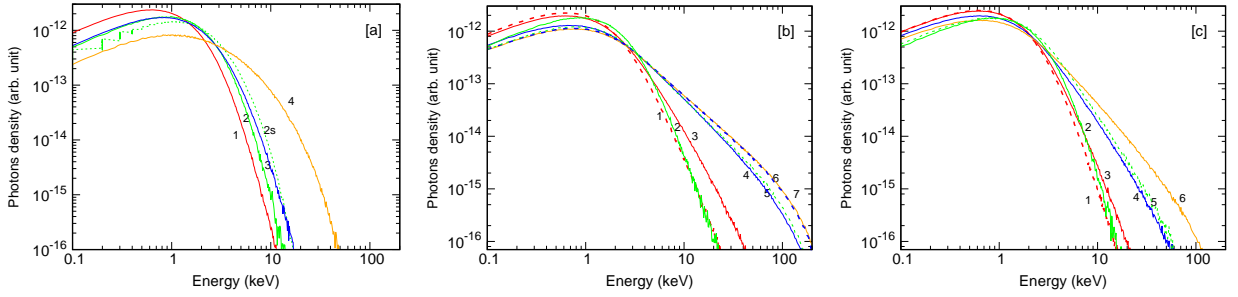


Figure 2: The simulated emergent spectra for different outflows geometry for a low medium temperature. The left is for collimated outflow, while middle and right panels are for case I and II of conical outflow respectively (see text). In left panel the curves 1,2,3 and 4 are for $\theta_b = 0$ (outflow), 180 (inflow), 90 and 90 degree respectively. The curve 2s is for the single scattering at $\theta_b = 180$ degree. In middle and right panel the curves 1,2,3,4,5 and 6 are for $\theta_b = 20, 160, 30, 60, 110$ and 90 degree respectively. In middle panel the curve 7 (dashed) is for 95 degree. The spectral parameters for all curves are $kT_e=3.0$ keV, $kT_b=0.5$ keV, $\tau = 3$ and $u_b = 0.45c$ except for the curve 4 of left panel where $\tau = 15$ and $u_b = 0.65c$.

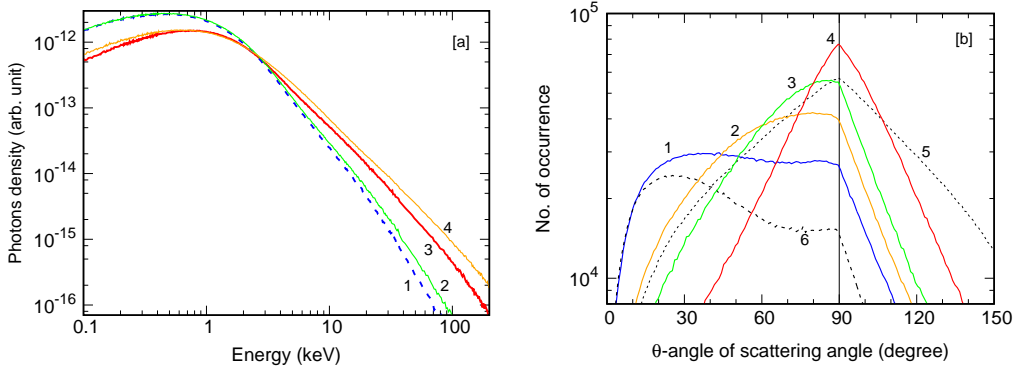


Figure 3: The left panel is for an emergent spectra for a high medium temperature ($kT_e = 30$ keV). The curve 3 is for a spectrum of TC dominated case ($(u_b/c)^2 \ll 3kT_e/(m_e c^2)$), while others are for bulk dominated case, $u_b = 0.75c$. The curve 1 is for collimated outflow of $\theta_b = 15$ degree, and the curves 2 and 4 are for conical outflow of $\theta_b = 15$ and 45 degree respectively. The right panel is for scattering angle distribution. Curves 1, 2, 3 and 4 are for conical outflow of $\theta_b = 15, 45, 60$ and 90 degree respectively and $u_b = 0.75c$, and the curve 6 is for $\theta_b = 15$ degree and $u_b = 0.85c$. The curve 5 is for TC dominated case. The rest parameters are $kT_b = 0.5$ keV and $\tau = 1$.

angle θ_b with axis perpendicular to the equatorial plane at scattering point P. The outflow direction will be any one of possible direction inside the cone from the P as shown in the right side of Figure 1. The torus temperature is T_e . Inside the torus the electron executes simultaneously thermal motion and bulk motion. The bulk motion is generally referred a movement in uni-direction, e.g., here collimated flow. However in conical outflow case, here the medium as a whole moves in upward direction but the electron's bulk motion direction is not unique as shown in the right side of Figure 1.

2.1 Results

To explore the general characteristics for BMC spectrum we consider a wide range of θ_b for both collimated and conical outflows. As our primary aim to explore HEP-tail of XRBs which observes in all spectral states, we consider a typical mid value of seed photon source temperature $kT_b = 0.5keV$. We take two different corona temperatures $kT_e = 3$ and $30 keV$, in which the low value may characterize the HS state and high value is for the LH state (e.g. Kumar & Misra, 2016b, references therein). As discussed, TC fails to generate observed HEP-tail, we consider only bulk motion dominated case or $(u_b/c)^2 \gg 3kT_e/(m_e c^2)$. Particularly, to determine the outflow direction for conical outflow geometry we consider two different plausible cases. In case I we simply consider, the outflow direction at scattering point P is in any one of directions on the surface of the cone from its vertex P, that is, $\theta_b = \text{constant}$ and ϕ_b varies from 0 to 2π (see right side of Figure 1). In case II, the outflow direction can be any one of directions within the conical region so here θ_b will vary from 0 to $\theta_b = \text{constant}$, and ϕ will vary again from 0 to 2π .

Emergent spectrum from Outflow geometry: The emergent spectra at low kT_e for collimated outflow are shown in Figure 2a for three different $\theta_b = 0$ (curve 1), 180 (curves 2 and 2s) and 90 (curves 3 and 4) degree. In which the curve 2s is for the single scattering and curve 4 is for the $\tau = 15$ and $u_b = 0.65c$. We do not find a high energy power-law tail in the collimated outflow even in the extreme condition (higher τ and larger u_b) like curve 4. Since, the seed photons direction is vertically upward, for first scattering the photon will collide head-on for $\theta_b = 180$ degree, and for $\theta_b = 0$ degree it will hit the electron from behind. The single scattered spectrum for $\theta_b = 180$ degree is harder than the spectrum for $\theta_b = 0$ degree. The Klein-Nishina cross section predicts that for relativistic electron the scattered photon will align in the incident electron direction (e.g., see Figure 3b). That is, for next scattering the photon will hit the electron from behind, therefore for multiple scattered BMC spectrum for $\theta_b = 180$ degree would be red-shifted from the single scattered spectrum. We find the same, see the curves 2 and 2s of Figure 2a (see also Janiuk et al., 2000).

In Figure 3a the curve 1 is for the emergent spectrum at large kT_e for collimated outflow with $\theta_b = 15$ degree and $u_b = 0.75c$. We notice a power-law tail in the spectrum. To confirm this we also compute the thermal Comptonized spectrum (or TC dominated spectrum i.e., $(u_b/c)^2 \ll 3kT_e/(m_e c^2)$) at same $kT_e = 30 keV$, which is shown by the curve 3. We find that in this case the collimated BMC spectrum for any θ_b is always softer in comparison to TC dominated one. Hence, in collimated outflow the power-law tail can be found for sufficiently large kT_e at where TC dominated spectrum has also power-law tail. The above results are consistent with Kylafis et al. (2014), where they described the power-law component in soft gamma-ray repeaters by BMC process with having a vertically downward bulk region onto the neutron star pole for a large kT_e . (see also Titarchuk et al., 2012, for a power-law component of gamma-ray burst spectrum).

Next, we compute the emergent spectrum of conical outflow at low kT_e , the results are shown in Figure 2b and Figure 2c for cases I and II respectively. We find, in general, the photon index decreases with θ_b for both cases, and the spectrum of case I is harder than the case II. Interestingly we find that to generate the power-law tails with $E_c > 200 keV$ and observed range of $\Gamma (> 2)$, the θ_b should be greater than 30 degree and $u_b > 0.4c$ (for low kT_e). Evidently, the case II is more plausible case for conical outflow in the system, however, for simplicity to extract the general picture, we consider the case I only. For large $kT_e (=30 keV)$, the emergent spectrum for case I with $u_b = 0.75c$ is shown in Figure 3a by curves 2 and 4 where $\theta_b = 15$ and 45 degree respectively. We find that the general trend of results is similar to the collimated case, i.e., when there is no HEP-tail for given θ_b at low kT_e then at large kT_e their spectrum is softer than the TC dominated spectrum. In another words, we find that for $\theta_b < 30$ degree, the Γ is higher from TC dominated one, while the opposite is true for the case of $\theta_b > 30$ degree.

Next to understand this distinction in details, in Figure 3b, the distribution of scattering angle (the angle between scattered and incident photon) has been shown for a conical outflow (case I). Here, the

Table 1: Sets of (outflow speed u_b , optical depth τ) and high energy cut-off E_c of bulk dominated BMC spectra of photon index $\Gamma \sim 2.5$ in conical outflow.

		$(u_b, \tau), E_c^a$ (MeV) when		
$kT_e =$	$\theta_b = 30^\circ$	$\theta_b = 45^\circ$	$\theta_b = 60^\circ$	
3keV	(0.8c, 5.2), 0.7	(0.72c, 2.0), 0.6	(0.6c, 1.9), 0.4	
	(0.85c, 4.2), 0.8	(0.85c, 1.2), 0.8	(0.7c, 1.2), 0.6	
30keV	(0.8c, 2.8), 1.1	(0.85c, 0.8), 1.2	(0.7c, 0.6), 0.8	
	(0.7c, 2.6), 0.8	(0.7c, 0.9), 0.8	(0.6c, 0.7), 0.6	

^a here, E_c increases with u_b (or kT_e) for given kT_e (or u_b); and for fixed value of E_c and θ_b , u_b and τ decrease by increasing kT_e .

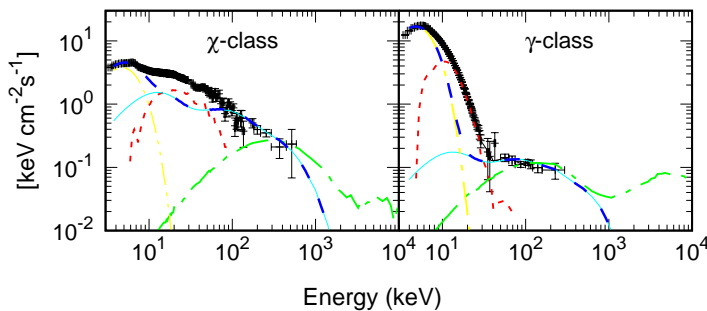


Figure 4: Comparison of the χ (left panel) and γ (right panel) classes of GRS 1915+105 with the bulk Comptonization model, here the data points are taken from [Zdziarski et al. \(2001\)](#). The two-dotted-dashed, solid, big-dashed, and short-dashed curves are for blackbody (BB), bulk Comptonization (BMC), BB + BMC, and residual (data-(BB+ BMC)) components respectively. Here, $\theta_b = 30$ degree, $u_b = 0.95c$, $kT_e = 3$ keV, $kT_b = 1.2$ keV and $\tau = 2.0$ (χ -class) = 2.8 (γ -class). Dotted-dashed curve is for BMC component when $u_b = 0.998c$ and $kT_e = 100$ keV, here the other components are not shown for clarity.

curves 1, 2, 3 and 4 are for $\theta_b = 15, 45, 60$ and 90 degree respectively with $u_b = 0.75c$ and curve 6 is for $\theta_b = 15$ degree and $u_b = 0.85c$. The curve 5 is for TC dominated case. We find that the scattered photons are in the outflow direction of electron and it tends to be more along a outflow direction for a large value of u_b (see curve 6). Since, in terms of the randomness the outflow direction becomes more random with increasing θ_b and it becomes completely random (like TC ones) when θ_b tends to 90 degree. We find a similar correspondence in terms of scattering angle, see the curves 4 and 5. Thus, it is expected here that after some value of θ_b the BMC spectrum becomes harder in comparison to the TC dominated one. We find here that for $\theta_b > 30$ degree the Γ is smaller in comparison to the TC one, and this is hold almost upto $u_b = 0.99c$. Since, BMC spectrum is degenerate over kT_e , u_b and τ . To illustrate this, in Table 1 we list the few ranges of these parameters along with E_c for a fixed typical photon index $\Gamma \sim 2.5$ for case I of conical outflow. We find, in general, the E_c increases with u_b for a given kT_e and θ_b .

Comparison with observations: In Figure 4 we compare qualitatively the observed HEP-tail of χ (LH) and γ (HS) classes of GRS 1915+105 with bulk Comptonized spectra at two values of $kT_e = 3$ and 100 keV for a conical outflow geometry of case I. The data points are taken from [Zdziarski et al. \(2001\)](#), see also for the parameters value for corresponding observation ID). The computed BMC spectrum for both classes are shown by cyan solid and green dotted-dashed curves for low and high kT_e respectively. We find that the BMC spectrum well describe the HEP-tail for both classes for both cases of kT_e . For completeness of spectral modeling, for low kT_e we also show the black body (BB, shown by yellow two-dotted-dashed curve), BB+BMC (blue big-dashed curve) and [data points - (BB + BMC)] (residual, shown by red short-dashed curve). In general the residual can be described either due to a relativistic

reflection spectra (e.g., Ross & Fabian, 2005) or due to TC component or both (e.g., McConnell et al., 2002; Farinelli et al., 2009; Revnivtsev et al., 2014; Kubota & Done, 2016). The spectral parameters set for low kT_e are $\theta_b = 30$ degree, $u_b = 0.95c$, $kT_b = 1.2\text{keV}$ and $\tau = 2.0$ (χ -class), 2.8 (γ -class). For high kT_e , the parameters are $\theta_b = 30$ degree, $u_b = 0.998c$, and $(kT_b, \tau) = (0.85\text{ keV}, 0.8)$ (for χ -class), $(0.35\text{ keV}, 3.0)$ (for γ -class).

As the HEP-tail is generated by BMC process with conical outflow geometry, like leptonic case of blazar radio jet, we assume that the hadrons do not contribute in the radiative process, the wind mechanical power is significantly due to the electrons, and the P_{wind} is (e.g., Zdziarski, 2014) $P_{wind} = \dot{M}_{wind}c^2 \left(\frac{1}{\sqrt{1-(u_b/c)^2}} \right)$, here \dot{M}_{wind} is the mass outflow rate $\dot{M}_{wind} = \Omega \mu m_e n_e R^2 u_b$, Ω ($= 2 \frac{\theta_b}{4\pi}$) is the covering factor, μ is the mean atomic weight, m_e is the mass of the electron, R is the launching radius and $n_e = \frac{\tau}{L\sigma_T}$ is electron density. For low kT_e , $\dot{M}_{wind} = 1.5 \times 10^{17}$ and $2.2 \times 10^{17} g/s$; $P_{wind} = 4.5 \times 10^{38}$ and $6.3 \times 10^{38} \text{erg/s}$ for χ - and γ -class respectively. For high kT_e , $\dot{M}_{wind} = 6.6 \times 10^{16}$ and $2.4 \times 10^{17} g/s$; $P_{wind} = 9.4 \times 10^{38}$ and $3.54 \times 10^{39} \text{erg/s}$ for χ - and γ -class respectively. Here we have considered the launching radius $R = 25R_g$, R_g is the gravitational radius and mass of BH of GRS 1915+105 (Reid et al., 2014) is $\sim 12M_\odot$.

The total luminosity for χ - and γ -class is 6.5×10^{38} , $1.7 \times 10^{39} \text{ erg/s}$ respectively (Zdziarski et al., 2001), however the intensity associated to the HEP-tail in χ -class is almost 35 times smaller than the total luminosity while almost 2 order smaller in case of γ -class. Hence, the kinetic power of wind P_{wind} is greater than the luminosity of HEP-tail. As the P_{wind} is calculated for $R = 25R_g$ or inner-region of the disk, the HEP-tail can be generated at the inner disk region. In addition, the HEP-tail flux of γ -class is almost 5 times fainter than χ -class (see Figure 4). And we find that the radio flux of γ -class is almost 3 times fainter than χ -class for this observation (see Figure 1 (1997 panel) and Figure 2 (1999 panel) of Rushton et al., 2010; see also (Muno et al., 2001; Fender et al., 1999)). With this similarity (which is also true in general) of HEP-tail and radio flux variation between two classes, we stress that the HEP-tail flux would be generated by the same population of electrons which generate radio emission. In other words the location of emission region of HEP-tail and radio is same on the disk. However, for concreteness of this result we have to consider a velocity distribution for bulk motion along with an appropriate magnetic configuration, which we will do in future work.

3 Summary

As it was noticed earlier that a spherically diverging outflow geometry is not a favourable ones to generate the high energy power-law tail by bulk Comptonization process (e.g. Laurent & Titarchuk, 2007), we investigate it with the different outflow geometry mainly a collimated (of angle θ_b) and conical outflow (of opening angle θ_b) from the accretion disk. The motivation for considering the outflow geometry is the similarity between the variation of HEP-tail flux in different spectral states and the variation of radio flux, e.g., the both radio and HEP-tail fluxes decrease when source moves from SPL to HS state. And the radio emission is generated by synchrotron emitting outflowing relativistic electron. In XRBs, the HEP-tail is identified in high energy bin ($E > 50\text{keV}$) with photon index $\Gamma > 2$ and energy cut-off $E_c > 200\text{keV}$. We have simulated the emergent BMC spectrum by a Monte Carlo scheme with considering, the seed photon source is on equatorial plane of the disk and inside the outflow region. For conical outflow, we have considered two different cases for outflow direction for electron, in case I it is in any one of the direction along the surface of the cone and in case II it is in any one of direction within the conic region.

For a low medium temperature, HEP-tail with observed range of Γ and E_c can not be generated in collimated outflow for any θ_b , but it can form in conical outflow when θ_b is greater than ~ 30 degree. At high medium temperature ($kT_e > 30\text{keV}$), the HEP-tail even generates in TC dominated spectrum, and it also finds in BMC spectrum either with collimated outflow or conical outflow for $\theta_b < 30\text{degree}$ but this BMC spectrum is softer than the TC dominated one. Particularly, in conical outflow, in general, the emergent spectrum of case I is harder than the case II, the Γ decreases with increasing θ_b . The BMC spectrum degenerates over parameters kT_e , u_b , τ (see equation (1)) and also θ_b (for conical outflow). For a fixed $\Gamma \sim 2.5$, we have explored the range of degenerate parameters and summarised it in Table 1.

In Fig. 4 we have qualitatively described the observed HEP-tail during χ - (LH) and γ -class (HS) of GRS 1915+105 for two values of $kT_e = 100$ and 3 keV (see Zdziarski et al., 2001 for the parameters value

for corresponding observation ID). We have found that for both values of kT_e the HEP-tail of either χ - or γ -class is well describe by BMC spectrum with conical outflow, and estimated u_b is relativistic. In addition, the requirement that the kinetic power of wind should be greater than the total luminosity of HEP-tail is also achieved at launching radius $\sim 25R_g$. Hence the HEP-tail can be generated at inner region of the disk. Combinedly with this result and observation features (meant, the HEP-tail flux changes in a similar way as the radio flux when source transits from one spectral state to another) we stress that the HEP-tail and radio flux can be generated at the same region with same relativistic electron distribution. Moreover, for few sources the polarization properties of HEP-tail has been measured (e.g., [Rodríguez et al., 2015](#), for crab pulsar e.g., [Vadawale et al., 2017](#)). Therefore, the present degeneracy in BMC spectrum may be lifted out by estimating its polarization properties, we will study this in future work.

Acknowledgement

Author is supported by University Grants Commission, New Delhi India through Dr. D.S. Kothari Post-Doctoral Fellowship (201718-PH/17-18/0013). Author acknowledges partial financial support from Indian Space Research Organisation (ISRO) with research Grant No. ISTC/PPH/BMP/0362. He wishes to thank Ranjeev Misra for valuable comments on this project and Banibrata Mukhopadhyay for their valuable suggestions and comments over the manuscript.

References

- Blandford R. D., Payne D. G., 1981a, [MNRAS](#), **194**, 1033
 Blandford R. D., Payne D. G., 1981b, [MNRAS](#), **194**, 1041
 Coppi P. S., 1999, in Poutanen J., Svensson R., eds, Astronomical Society of the Pacific Conference Series Vol. 161, High Energy Processes in Accreting Black Holes. p. 375 ([arXiv:astro-ph/9903158](#))
 Degenaar N., et al., 2016, [MNRAS](#), **461**, 4049
 Díaz Trigo M., Boirin L., 2016, [Astronomische Nachrichten](#), **337**, 368
 Done C., Kubota A., 2006, [MNRAS](#), **371**, 1216
 Done C., Gierliński M., Kubota A., 2007, [A&A Rev.](#), **15**, 1
 Drappeau S., et al., 2017, [MNRAS](#), **466**, 4272
 Farinelli R., Paizis A., Landi R., Titarchuk L., 2009, [A&A](#), **498**, 509
 Fender R., Belloni T., 2012, [Science](#), **337**, 540
 Fender R. P., Hendry M. A., 2000, [MNRAS](#), **317**, 1
 Fender R. P., Kuulkers E., 2001, [MNRAS](#), **324**, 923
 Fender R. P., Garrington S. T., McKay D. J., Muxlow T. W. B., Pooley G. G., Spencer R. E., Stirling A. M., Waltman E. B., 1999, [MNRAS](#), **304**, 865
 Fender R. P., Belloni T. M., Gallo E., 2004, [MNRAS](#), **355**, 1105
 Fender R. P., Homan J., Belloni T. M., 2009, [MNRAS](#), **396**, 1370
 Ghosh H., Garain S. K., Chakrabarti S. K., Laurent P., 2010, [International Journal of Modern Physics D](#), **19**, 607
 Gierliński M., Zdziarski A. A., Poutanen J., Coppi P. S., Ebisawa K., Johnson W. N., 1999, [MNRAS](#), **309**, 496
 Homan J., Neilsen J., Allen J. L., Chakrabarty D., Fender R., Fridriksson J. K., Remillard R. A., Schulz N., 2016, [ApJ](#), **830**, L5
 Janiuk A., Czerny B., Życki P. T., 2000, [MNRAS](#), **318**, 180
 Knigge C., Woods J. A., Drew J. E., 1995, [MNRAS](#), **273**, 225
 Kubota A., Done C., 2016, [MNRAS](#), **458**, 4238
 Kumar N., Misra R., 2016a, [MNRAS](#), **461**, 4146
 Kumar N., Misra R., 2016b, [MNRAS](#), **461**, 2580
 Kylafis N. D., Trümper J. E., Ertan Ü., 2014, [A&A](#), **562**, A62
 Laurent P., Titarchuk L., 1999, [ApJ](#), **511**, 289
 Laurent P., Titarchuk L., 2007, [ApJ](#), **656**, 1056

- McClintock J. E., Remillard R. A., 2006, Black hole binaries. Lewin, W. H. G. and van der Klis, M., pp 157–213, [doi:10.1017/CBO9780511536281](https://doi.org/10.1017/CBO9780511536281)
- McConnell M. L., et al., 2002, *ApJ*, **572**, 984
- Miller J. M., et al., 2016, *ApJ*, **821**, L9
- Motta S., Belloni T., Homan J., 2009, *MNRAS*, **400**, 1603
- Muno M. P., Remillard R. A., Morgan E. H., Waltman E. B., Dhawan V., Hjellming R. M., Pooley G., 2001, *ApJ*, **556**, 515
- Niedźwiecki A., Zdziarski A. A., 2006, *MNRAS*, **365**, 606
- Ponti G., Fender R. P., Begelman M. C., Dunn R. J. H., Neilsen J., Coriat M., 2012, *MNRAS*, **422**, L11
- Psaltis D., 2001, *ApJ*, **555**, 786
- Reid M. J., McClintock J. E., Steiner J. F., Steeghs D., Remillard R. A., Dhawan V., Narayan R., 2014, *ApJ*, **796**, 2
- Revnivtsev M. G., Tsygankov S. S., Churazov E. M., Krivonos R. A., 2014, *MNRAS*, **445**, 1205
- Rodriguez J., et al., 2015, *ApJ*, **807**, 17
- Ross R. R., Fabian A. C., 2005, *MNRAS*, **358**, 211
- Rushton A., Spencer R. E., Pooley G., Trushkin S., 2010, *MNRAS*, **401**, 2611
- Sazonov S. Y., Sunyaev R. A., 2000, *A&A*, **354**, L53
- Tetarenko B. E., Lasota J.-P., Heinke C. O., Dubus G., Sivakoff G. R., 2018, *Nature*, **554**, 69
- Titarchuk L., Shaposhnikov N., 2010, *ApJ*, **724**, 1147
- Titarchuk L., Mastichiadis A., Kylafis N. D., 1997, *ApJ*, **487**, 834
- Titarchuk L., Farinelli R., Frontera F., Amati L., 2012, *ApJ*, **752**, 116
- Tombesi F., Tazaki F., Mushotzky R. F., Ueda Y., Cappi M., Gofford J., Reeves J. N., Guainazzi M., 2014, *MNRAS*, **443**, 2154
- Tombesi F., Meléndez M., Veilleux S., Reeves J. N., González-Alfonso E., Reynolds C. S., 2015, *Nature*, **519**, 436
- Vadawale S. V., et al., 2017, *Nature Astronomy*, pp 1–6
- Zdziarski A. A., 2014, *MNRAS*, **445**, 1321
- Zdziarski A. A., Grove J. E., Poutanen J., Rao A. R., Vadawale S. V., 2001, *ApJ*, **554**, L45
- Zhang H., Yu W., 2015, *MNRAS*, **451**, 1740

A Monte Carlo Method

As discussed, we considered a torus shaped Comptonizing medium (see Figure 1), in which τ is defined in the vertical direction. The electron density n_e inside the medium is $n_e = \frac{\tau}{L\sigma_T}$, here σ_T is the Thomson cross section. In BMC process the electrons possess a bulk velocity in addition to the thermal velocity. In moving media the mean free path of the photons λ exceeds that in static medium, and it is taken into account (e.g., [Sazonov & Sunyaev, 2000](#)). We compute the BMC spectrum using the MC method. The algorithm for MC code is similar to that of [Kumar & Misra \(2016a\)](#) for a thermal Comptonization and we have extended it for BMC process by including the bulk (outflow) motion as discussed by [Laurent & Titarchuk \(1999\)](#); [Niedźwiecki & Zdziarski \(2006\)](#) by neglecting general relativistic effects. Generally, in MC calculation, a photon is tracked till it leaves the medium after either single or multiple or without scattering. This process is repeated for a large number of photons to obtain the statistically significant results, like an emergent spectrum. The important steps involved in MC calculation are described as follows.

- In first step, we obtain the incident photon’s energy $E = h\nu$ from a black body distribution at temperature T_b , and the electron’s thermal velocity from the velocity distribution of temperature T_e . We fix the corona boundary of width W and height L at radius r as shown in Figure 1. We consider an isotropic distribution for the photons and electron’s thermal velocity direction inside the corona. We determine the outflow direction of electron as describe in Figure 1, and take electron’s bulk speed u_b . The λ of photon of energy E is computed for a given n_e (or τ), T_e , and u_b . We compute the above quantities in global coordinate fixed at centre of torus (or at the compact object).

- Next, we obtain the collision free path of the photon l_f inside the corona using an exponential pdf (probability distribution function), $\exp\left(\frac{-l_f}{\lambda}\right)$, and find the scattering point P position in the global coordinate. Further we determine the condition for occurrence of scattering at P. If the point P is inside the corona then the scattering will happen otherwise the photon will escape the corona without scattering.
- In second step we transform the quantities from global coordinate to the comoving frame of electron's bulk velocity. By knowing the angle between photon's direction and electron's bulk velocity, we determine the Doppler boosted frequency and aberration for photon in comoving frame.
- In third step to describe the Compton scattering, we transform the quantities from comoving frame to the electron rest frame (as in comoving frame, the electron has only thermal velocity). By knowing the angle between photon's direction and electron's thermal velocity in comoving frame, we determine the Doppler boosted frequency and aberration for photon in rest frame.
- Using Klein-Nishina cross section $\left(\frac{1}{4}r_o^2\left(\frac{k'}{k}\right)^2\left[\frac{k}{k'} + \frac{k'}{k} - \sin^2\theta\right]\right)$, here $k = \frac{h\nu}{c}$ is the incident photon momentum, $k' = \frac{h\nu'}{c}$ is the scattered photon momentum, ν and ν' are incident and scattered photon frequency respectively, r_o is the classical radius of the electron, θ is the scattering angle), we extract the scattering angle. Using Compton scattering frequency formula $\left(\frac{\nu'}{\nu} = \frac{1}{1 + \frac{h\nu}{m_e c^2}(1 - \cos\theta)}\right)$ in electron rest frame we compute the scattered photon frequency.
- Next we find the scattered photon's direction in electron rest frame. We transform back the quantities (frequency of scattered photon and its aberration) from electron rest frame to the comoving frame. We find the scattered photon's direction in comoving frame. Finally we compute the scattered photon's frequency and its direction in global coordinate by transforming back the quantities from comoving frame to the global coordinate (or lab frame).
- Next we compute the collision free distance l_f for the scattered photon (of energy $E' = h\nu'$) and find the next scattering point P' position. If the P' lies inside the corona then next scattering will occur otherwise photon will escape the medium.
- For next scattering we proceed the calculations with treating k' of previous scattering as an incident photon, and follow the same steps till the scattered photon escapes the medium.

A.1 MC results verification

As discussed in method section §2 we check here the MC code by comparing the simulated bulk Comptonized spectrum to thermal Comptonized one for those parameters sets which have same ΔE , for example, the sets $(kT_e = 3 \text{ keV}, u_b = 0)$ for TC and $(kT_e = 2 \text{ keV}, u_b = 0.0766c)$ for BMC; here we neglect the term $\frac{4u_b}{c\tau}$ in calculation of ΔE . We find that the emergent spectra for both sets are identical for either single, or multiple scattering or Wien peak spectrum (for large $\langle N_{sc} \rangle \sim 500$) which are shown by curves 1, 2 and 3 in Figure 5 respectively.

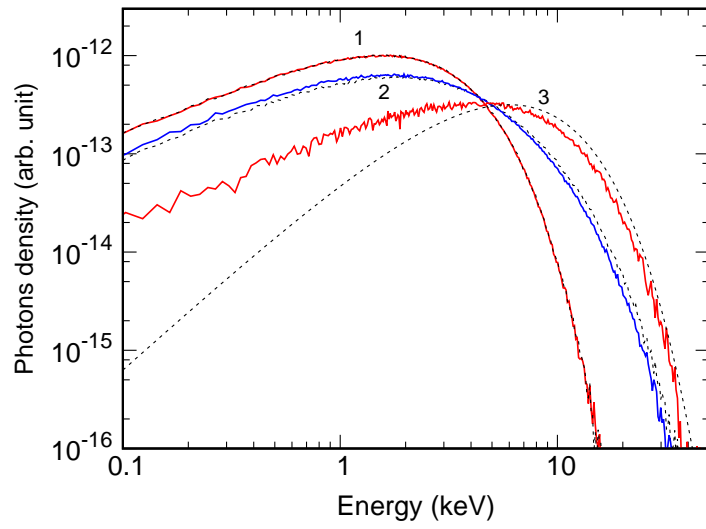


Figure 5: Spectra comparing Monte Carlo results. The solid lines are for bulk Comptonization ($kT_e = 2$ keV, $u_b=0.0766c$) and dashed lines are for thermal Comptonization ($kT_e = 3$ keV, $u_b=0.0$). The curves 1, 2, and 3 are for single scattering, multiple scattering ($\langle N_{sc} \rangle \sim 46$), and Wien peak ($\langle N_{sc} \rangle > 500$) respectively.